

Available online at [www.sciencedirect.com](http://www.sciencedirect.com)

ScienceDirect

journal homepage: [www.elsevier.com/locate/AJPS](http://www.elsevier.com/locate/AJPS)

## Research Article

# Acidic/hypoxia dual-alleviated nanoregulators for enhanced treatment of tumor chemo-immunotherapy



Xiaoju Guo<sup>a,b,1</sup>, Xiaoxiao Chen<sup>b,d,1</sup>, Jiayi Ding<sup>b</sup>, Feng Zhang<sup>b</sup>, Shunyang Chen<sup>a,b</sup>, Xin Hu<sup>a,b</sup>, Shiji Fang<sup>b,c</sup>, Lin Shen<sup>b</sup>, Chenying Lu<sup>a,b,c,d</sup>, Zhongwei Zhao<sup>a,b,c,d</sup>, Jianfei Tu<sup>a,b,c,d</sup>, Gaofeng Shu<sup>b,d,\*</sup>, Minjiang Chen<sup>b,d,\*</sup>, Jiansong Ji<sup>a,b,c,d,\*</sup>

<sup>a</sup>Lishui Central Hospital, Shaoxing University, Shaoxing 312000, China

<sup>b</sup>Zhejiang Key Laboratory of Imaging and Interventional Medicine, Imaging Diagnosis and Interventional Minimally Invasive Institute, The Fifth Affiliated Hospital of Wenzhou Medical University, Lishui 323000, China

<sup>c</sup>Clinical College of The Affiliated Central Hospital, School of Medicine, Lishui University, Lishui 323000, China

<sup>d</sup>Key Laboratory of Precision Medicine of Lishui, Lishui 323000, China

## ARTICLE INFO

## Article history:

Received 22 November 2023

Revised 2 February 2024

Accepted 17 February 2024

Available online 16 March 2024

## Keywords:

CaCO<sub>3</sub>-based nanoparticles

Hypoxia attenuation

Acidity neutralization

Reversal of chemotherapy

resistance

Enhanced chemo-immunotherapy

## ABSTRACT

Chemotherapy plays a crucial role in triple-negative breast cancer (TNBC) treatment as it not only directly kills cancer cells but also induces immunogenic cell death. However, the chemotherapeutic efficacy was strongly restricted by the acidic and hypoxic tumor environment. Herein, we have successfully formulated PLGA-based nanoparticles concurrently loaded with doxorubicin (DOX), hemoglobin (Hb) and CaCO<sub>3</sub> by a CaCO<sub>3</sub>-assisted emulsion method, aiming at the effective treatment of TNBC. We found that the obtained nanomedicine (DHCaNPs) exhibited effective drug encapsulation and pH-responsive drug release behavior. Moreover, DHCaNPs demonstrated robust capabilities in neutralizing protons and oxygen transport. Consequently, DHCaNPs could not only serve as oxygen nanoshuttles to attenuate tumor hypoxia but also neutralize the acidic tumor microenvironment (TME) by depleting lactic acid, thereby effectively overcoming the resistance to chemotherapy. Furthermore, DHCaNPs demonstrated a notable ability to enhance antitumor immune responses by increasing the frequency of tumor-infiltrating effector lymphocytes and reducing the frequency of various immune-suppressive cells, therefore exhibiting a superior efficacy in suppressing tumor growth and metastasis when combined with anti-PD-L1 ( $\alpha$ PD-L1) immunotherapy. In summary, this study highlights that DHCaNPs could effectively attenuate the acidic and hypoxic TME, offering a promising strategy to figure out an enhanced chemo-immunotherapy to benefit TNBC patients.

© 2024 Published by Elsevier B.V. on behalf of Shenyang Pharmaceutical University.

This is an open access article under the CC BY-NC-ND license

(<http://creativecommons.org/licenses/by-nc-nd/4.0/>)

\* Corresponding authors.

E-mail addresses: [shugf1208@gmail.com](mailto:shugf1208@gmail.com) (G. Shu), [minjiangchenv@163.com](mailto:minjiangchenv@163.com) (M. Chen), [jjstcty@wmu.edu.cn](mailto:jjstcty@wmu.edu.cn) (J. Ji).

<sup>1</sup> These authors contributed equally to this work.

Peer review under responsibility of Shenyang Pharmaceutical University.

## 1. Introduction

Breast cancer is the most frequently diagnosed malignancy and the leading cause of cancer-associated mortality among women worldwide [1,2]. According to the latest data, approximately 2.26 million new cases of breast cancer are diagnosed globally, leading to over 680,000 patient deaths [3]. Approximately 15%–25% of breast cancer cases are diagnosed as triple-negative breast cancer (TNBC), which is characterized by the absence of progesterone (PR), estrogen (ER), and human epidermal growth factor (HER2) receptor expression on the membranes of tumor cells [4,5]. Moreover, TNBC is notable for its pronounced cellular invasiveness and a marked tendency for visceral metastasis to various organs, which typically lead to a lower survival rate compared to other breast cancer subtypes [5]. Despite noteworthy progress in therapeutic strategies, the 5-year survival rate for patients with metastatic TNBC remains dismally low at only 12% [6,7].

In clinical practice, chemotherapy has been recognized as a crucial therapeutic intervention for various types of human cancers, including TNBC [8–10]. Beyond the direct cytotoxic effects on cancer cells, chemotherapy has the potential to potentiate certain levels of anticancer immune responses by inducing immunogenic cell death (ICD) [11,12]. ICD triggers the release of damage-associated molecular patterns (DAMPs), such as adenosine triphosphate (ATP), calreticulin (CRT), and high mobility group protein B1 (HMGB1) [13,14]. These DAMPs are crucial in advancing dendritic cells (DCs) maturation and antigen presentation, leading to T cell activation [15,16]. This process further stimulates the deployment of cytotoxic T lymphocytes (CTLs) to the tumor, thereby amplifying tumor-specific cellular immunity. As a result, a rational strategy involving the strategic utilization of chemotherapy alongside immune checkpoint blockade (ICB) therapy has emerged to enhance the therapeutic efficacy in inhibiting the progression of both local tumors and tumor metastasis [17–20]. However, the tumor microenvironment (TME) can significantly diminish the cytotoxic effects of chemotherapeutic agents while also limiting the response rates of immune ICB therapy [21,22]. Hence, there is a critical demand to formulate strategies capable of reversing the immune-suppressive TME while concurrently triggering a potent antitumor immune response. These efforts are essential to achieve enhanced chemo-immunotherapy of cancers.

It is well known that tumor acidity and tumor hypoxia stand as two characteristic microenvironmental features prevalent in almost all solid tumors. Recent studies have found that lactic acid, a byproduct of glycolysis, is closely linked to the cellular metabolic alterations, aberrant tumor angiogenesis, and cancer metastasis [23,24]. Moreover, lactic acid has the potential to substantially reduce the cellular uptake of weakly basic drugs such as doxorubicin (DOX), thus contributing to the emergence of chemoresistance [25,26]. Similarly, the tumor hypoxic microenvironment can significantly diminish the anticancer efficacy of chemotherapy through different mechanisms: (i) Hypoxic microenvironment fosters the abnormal vascularization, leading to a diminished availability of drugs [27]; (ii) Hypoxic microenvironment can significantly upregulate the levels

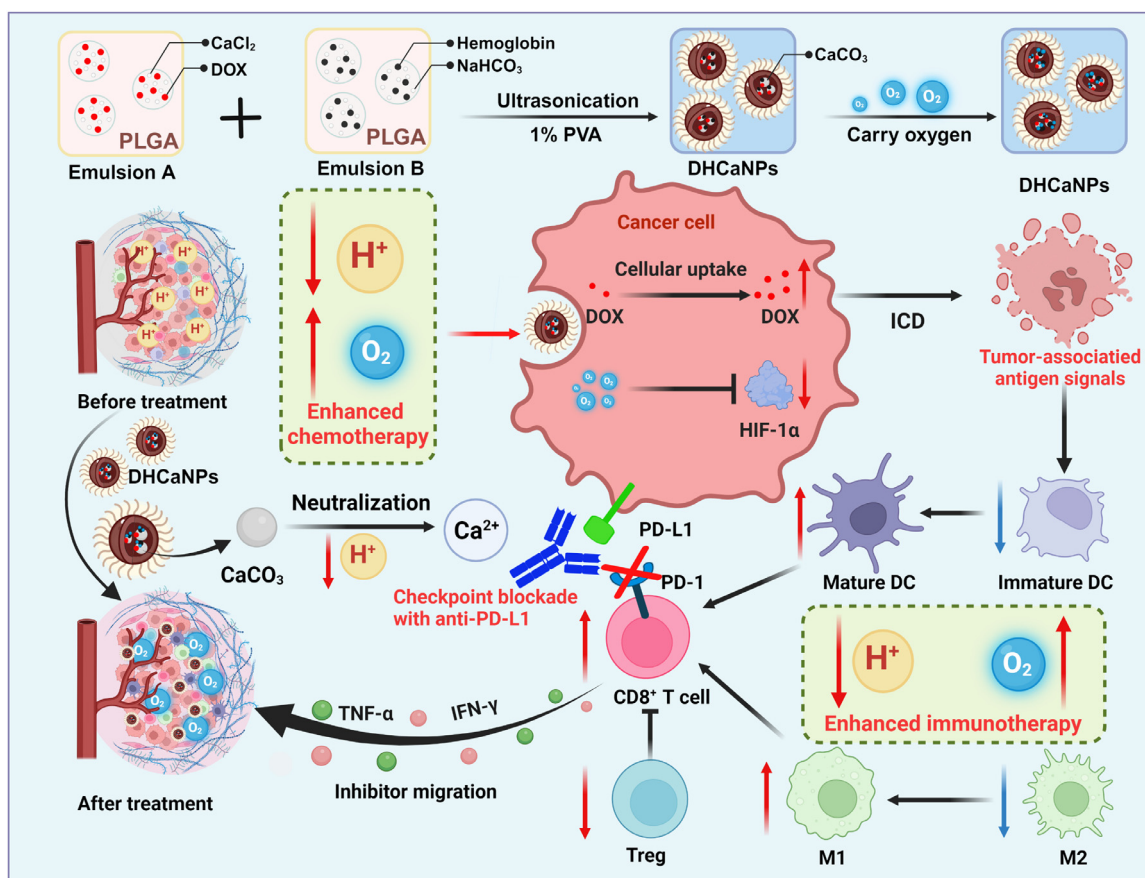
of hypoxia-inducible factor-1 $\alpha$  (HIF-1 $\alpha$ ), thereby governing a multitude of genes involved in the regulation of tumor growth, metastasis, angiogenesis, and therapeutic resistance [28,29]. Besides, growing evidence has underscored that the acidic and hypoxic TME plays a role in diminishing and inducing apoptosis of tumor-killing effector lymphocytes, while also facilitating the infiltration of immunosuppressive immune cells within tumors [30–32]. Hence, we postulated that the concurrent alleviation of tumor acidity and hypoxia could significantly increase the chemotherapeutic sensitivity and modulate the immunosuppressive TME, thereby greatly enhancing the therapeutic effectiveness of chemo-immunotherapy.

Calcium carbonate (CaCO<sub>3</sub>) is a water-insoluble alkaline biomaterial that can effectively react with proton under acidic conditions. Therefore, CaCO<sub>3</sub> is an effectively proton neutralizing agent, capable of continuously modulating the acidic TME [26]. Hemoglobin (Hb) is an intrinsic protein found in red blood cells, which plays a pivotal role in transporting oxygen to bodily tissues. It possesses the capacity to reversibly attach to four molecules of oxygen, making it an indispensable component in oxygen-enriched chemotherapy as a biocompatible oxygen carrier [33]. Herein, in this study, a poly (D, lactide-co-glycolide) (PLGA)-based nanoparticle incorporated with DOX, Hb and CaCO<sub>3</sub> was prepared as a novel nanopatform (abbreviated as DHCaNPs) for amplified chemo-immunotherapy of TNBC. By harnessing the versatile molecular adsorption capability of CaCO<sub>3</sub>, DHCaNPs could encapsulate DOX and Hb more effectively than their counterparts lacking CaCO<sub>3</sub>. In addition, DHCaNPs exhibited a pH-dependent drug release profile, offering advantageous prospects for cancer treatment. Due to the presence of CaCO<sub>3</sub> and Hb, DHCaNPs demonstrated an excellent capability of simultaneously alleviating tumor acidity and hypoxia, thereby greatly enhancing the therapeutic efficacy of chemotherapy against TNBC. Meanwhile, DHCaNPs could effectively elicit systemic antitumor immune responses as evidenced by increased frequency of tumor-infiltrating effector lymphocytes and reduced frequency of various immune-suppressive cells. Therefore, the combination treatment of DHCaNPs and anti-PD-L1 ( $\alpha$ PD-L1) was shown to be capable of effectively suppressing the growth of primary and metastatic tumors (Scheme 1). Overall, our study presents the formulation of DHCaNPs to modulate tumor hypoxic and acidic microenvironments, which could remarkably enhance the chemo-immunotherapy of TNBC.

## 2. Materials and methods

### 2.1. Materials

Polyvinyl alcohol (PVA), doxorubicin hydrochloride (DOX-HCl), Hb, sodium bicarbonate (NaHCO<sub>3</sub>), calcium chloride (CaCl<sub>2</sub>), dichloromethane (DCM), dimethyl sulfoxide (DMSO) and indocyanine green (ICG) were purchased from Aladdin Chemicals Co., Ltd. (Shanghai, China). PLGA was acquired from Sigma-Aldrich Inc., St Louis, MO, USA. Polyethylene glycol-poly lactic acid-co-glycolic acid (PEG-PLGA) was acquired from ToYong Biotech. Inc. (Shanghai, China).



**Scheme 1 – Schematic illustration of DHCaNPs for amplified chemo-immunotherapy of TNBC.**

Hypoxyprobe<sup>TM</sup>-1 plus kit was acquired from Hypoxyprobe Inc., Burlington MA, USA. SNARF<sup>TM</sup>-4F 5-(and-6)-carboxylic acid (S23920) was purchased from Thermo Fisher Scientific. (Waltham, USA). Annexin V-FITC apoptosis detection kit, 3-(4,5-dimethyl-2-thiazolyl)-2,5-diphenyl-2-H-tetrazolium bromide (MTT), Bicinchoninic Acid (BCA) protein assay kit, Calcein AM/PI cell viability/cytotoxicity assay kit, 2',7'-bis-(2-carboxyethyl)-5-(and-6)-carboxyfluorescein (BCECF) were purchased from Beyotime Biotechnology Co., Ltd. (Shanghai, China). Anti-HIF-1 $\alpha$  antibody was purchased from Abcam, Cambridge, UK. Antibodies for flow cytometry assays including APC anti-mouse CD3 antibody, FITC anti-mouse CD4 antibody, PE anti-mouse CD8a antibody PE anti-mouse Foxp3 antibody, FITC anti-mouse CD11c antibody APC anti-mouse CD80 antibody PE anti-mouse CD86 antibody PE anti-mouse CD206 antibody, PerCP/Cyanine5.5 anti-mouse CD11b antibody, FITC anti-mouse F4/80 antibody were acquired from BioLegend, Inc. (San Diego, CA, USA). ELISA kits including tumor necrosis factor- $\alpha$  (TNF- $\alpha$ ) and interferon- $\gamma$  (IFN- $\gamma$ ) were purchased from Jiangsu Enzyme-free Industrial Co., Ltd. (Jiangsu, China).  $\alpha$ PD-L1 (B7-H1) was purchased from Bio Cell (USA).

## 2.2. Cell lines and animals

The murine 4T1 breast cancer cells were purchased from American Type Culture Collection (Rockville, MD, USA). The

4T1 cells were cultured in RPMI 1640 medium supplemented with 10% (v/v) FBS and penicillin/streptomycin (100 U/ml of each), and maintained in a cell incubator at 37 °C with 5% CO<sub>2</sub>. In some experiments, the culture medium was added with 10 mM lactic acid to mimic the acidic condition. The hypoxic condition was induced using a hypoxia incubator with conditions set at 2% O<sub>2</sub>, 5% CO<sub>2</sub>, and 93% N<sub>2</sub>.

BALB/c female mice (6–8 weeks, 20–25 g) were acquired from Shanghai Silaike Laboratory Animal Co., Ltd (Shanghai, China). All animal procedures were performed in accordance with the Guidelines for Care and Use of Laboratory Animals of Lishui University and approved by the Animal Ethics Committee of Lishui University. The unilateral subcutaneous tumor-bearing murine models were inoculated by injecting 4T1 cells into the right armpit of the mice. The bilateral subcutaneous tumor-bearing murine models were inoculated by injecting 4T1 cells into their right and left flanks at Day 7 and 3, respectively.

## 2.3. Preparation of DHCaNPs

DHCaNPs was prepared by a CaCO<sub>3</sub>-assisted double emulsion method as described in a previous study [34]. In brief, two water-in-oil (W/O) emulsions (A, B) were firstly prepared by probe sonication method. Emulsion A was prepared by emulsifying 250  $\mu$ l CaCl<sub>2</sub> aqueous solution (1.25 M, with 1 mg

DOX) with 750  $\mu$ l DCM solution (15 mg/ml PLGA, 15 mg/ml PLGA-PEG) using a probe sonicator (99 pulses, pulse on: 3 s, pulse off: 7 s). Emulsion B was prepared by emulsifying 250  $\mu$ l NaHCO<sub>3</sub> aqueous solution (0.625 M, with 5 mg Hb) with 750  $\mu$ l DCM solution (15 mg/ml PLGA, 15 mg/ml PLGA-PEG) via the same probe sonication method. Subsequently, emulsion A and emulsion B were mixed and sonicated for 99 pulses using the same parameters to formulate emulsion C. Afterwards, water-in-oil-in-water (W/O/W) emulsion was prepared by dropwise adding emulsion C into 3 ml PVA solution (1%, w/w) under a water bath sonicator for 5 min. The obtained W/O/W emulsion was allowed to stir at ambient temperature for 6 h to evaporate DCM. Finally, the as-prepared DHCaNPs was washed 3 times with distilled water via high-speed centrifugation (21,000 g, 10 min) to remove the unencapsulated DOX and Hb, followed by removing the unwanted large aggregates via mild centrifugation (900 g, 3 min). The other control nanoparticles (HCaNPs, DHCaNPs and DHNPs) used in this study were prepared by the same procedure apart from introducing different corresponding components.

#### 2.4. Characterization of DHCaNPs

The morphology of DHCaNPs was examined using a transmission electron microscope (TEM, FEI Talos F200s, USA). The size and size distribution of DHCaNPs were assessed using a laser diffraction particle size analyzer (Zetasizer Lab, UK). The UV-VIS-NIR absorption spectrum of DHCaNPs was recorded using a microplate reader (Tecan Infinite M200 PRO). The amount of DOX in the supernatants subsequent to DHCaNPs preparation was quantified by measuring the UV-Vis-NIR absorbance value at 480 nm, followed by calculating the encapsulation efficiency (EE) and drug loading (DL) of DOX. Similarly, the EE and DL of DHCaNPs for Hb were determined by quantifying the amount of Hb in the supernatants after the nanoparticle preparation using BCA assay.

The proton neutralization capacity of DHCaNPs was assessed by monitoring the pH changes of DHCaNPs suspensions under acidic conditions. In brief, an acidic solution with a pH of approximately 6.5 was firstly prepared by adding diluted HCl to 5 ml phosphate-buffered saline (PBS) solution. Then, the pH changes of acidic solution as a function of time were recorded after the induction of DHCaNPs (final nanoparticle concentration: 2 mg/ml) using a digital pH meter (Mettler-Toledo Instruments Co., Ltd., Shanghai, China). The counterpart of DHCaNPs (DHNPs, without CaCO<sub>3</sub>) was employed as a control group.

The oxygen-carrying capacity of DHCaNPs was assessed by monitoring the changes in the dissolved oxygen concentration of DHCaNPs suspensions. In brief, 1 ml DHCaNPs nanosuspension containing 15 mg/ml Hb was treated with oxygen bubbling for 3 min. Then, the oxygen-saturated DHCaNPs nanosuspension was added into 4 ml oxygen-free aqueous solution. Afterward, the oxygen evolution dynamics were monitored using a dissolved oxygen meter (Rex, JPB-607A, China).

#### 2.5. pH-responsive drug release of DHCaNPs

The drug release behavior of DHCaNPs was studied by dialysis bag method. In brief, a known amount of DHCaNPs nanosuspensions (DOX = 0.5 mg/ml) was placed into a dialysis bag (MWCO 3500 Da) and subsequently dialyzed against PBS solutions with varying pH values (pH 7.4, 6.5 and 5.0), all while maintaining a continuous agitation at 100 rpm and a temperature of 37 °C. At specific intervals, a fresh buffer solution with the same pH value was introduced following the collection of 5 ml of the released medium. The concentration of DOX in the released medium was quantified by UV-Vis-NIR method. The absorbance of the released medium at 480 nm was quantified, and the concentration of DOX was determined by employing a calibration curve, which was generated using PBS containing varying concentrations of standard DOX. Then, the cumulative drug release profile was calculated based on the concentration of DOX in the released medium collected in each timepoint.

#### 2.6. In vitro cytotoxicity of DHCaNPs

In vitro cytotoxicity of DHCaNPs towards 4T1 cells was evaluated by MTT assay. In brief, 4T1 cells were cultured in a 96-well plate at a density of  $1 \times 10^4$  cells per well. After 12 h incubation, the cells were exposed to varying doses of DHCaNPs for 48 h. Subsequently, 20  $\mu$ l MTT solution (5 mg/ml) was introduced to each well, which was incubated for an additional 4 h. Following removal of the medium, the resultant purple formazan product was solubilized in DMSO for 15 min. The absorbance of each sample was then measured at 570 nm utilizing an automated microplate reader. Then, the viabilities of 4T1 cells treated with DHCaNPs under normal, acidic or hypoxic conditions were calculated using the following formula:

$$\text{Cell viability (\%)} = \frac{\text{Abs}_{\text{test cells}}}{\text{Abs}_{\text{control cells}}} \times 100\%$$

Subsequently, the cell viability of 4T1 cells treated with DHCaNPs was also visibly evaluated by Calcein AM/PI cell viability/cytotoxicity assay. In brief, 4T1 cells cultured in normal, acidic or hypoxia conditions were initially exposed DHCaNPs or other formulations a dosage of 3  $\mu$ g/ml DOX for 48 h. Subsequently, the cells were stained with Calcein AM/PI for 30 min at 37 °C. Following treatment, the live/dead cell fluorescent images were captured using a fluorescence microscope (DMi8, Leica, Germany).

Moreover, the ability of DHCaNPs to induce cell apoptosis under normal, acidic or hypoxic conditions was evaluated by flow cytometry. Briefly, 4T1 cells were cultured in 12-well plates at a density of  $1 \times 10^5$  cells per well overnight, and they were subsequently treated with DHCaNPs or other formulations a dosage of 3  $\mu$ g/ml DOX for 48 h. Then, the cells were harvested and stained with Annexin V-FITC/PI apoptosis detection kit. Then, the percentage of apoptotic cells in each group were analyzed by flow cytometry (BD FACSCanto, BD Biosciences, USA).

## 2.7. Cellular uptake analysis

The cellular uptake behavior of DHCaNPs under normal, acidic, or hypoxic conditions was initially evaluated using a confocal laser scanning microscope (CLSM, STELLARIS 5, Leica, Germany). Briefly, 4T1 cells were cultured in 12-well plates at a density of  $1 \times 10^5$  cells per well overnight, and they were subsequently treated with DHCaNPs or other formulations (DOX = 2  $\mu\text{g}/\text{ml}$ ) for 12 h. Then, the cells were washed, fixed, and stained with DAPI. Following treatment, fluorescent images of cells in each group were captured by CLSM. Additionally, the DOX fluorescence intensity of cells exposed to DHCaNPs or other formulations under the same aforementioned conditions was quantified using flow cytometry.

## 2.8. In vitro acidity and hypoxia alleviation

The ability of DHCaNPs to alleviate tumor acidity at cellular level was evaluated by using BCECF as an intracellular pH-responsive fluorescent probe. In brief, 4T1 cells were cultured in 12-well plates at a density of  $1 \times 10^5$  cells per well overnight. The normal or acidic cells were then exposed to DHCaNPs or other formulations (DOX = 2  $\mu\text{g}/\text{ml}$ ) for 12 h. Subsequently, the cells were stained with BCECF following the manufacturer's protocol. The fluorescent images of cells in each group were observed under a fluorescence microscope. Moreover, the pH values of culture medium were detected by a pH microelectrode.

The ability of DHCaNPs to alleviate tumor hypoxia at cellular level was initially evaluated by using pimonidazole as a hypoxia probe. In brief, 4T1 cells were cultured in 12-well plates at a density of  $1 \times 10^5$  cells per well overnight. The normal or hypoxic cells were then exposed to DHCaNPs or other formulations (DOX = 2  $\mu\text{g}/\text{ml}$ ) for 12 h. Subsequently, the cells were stained with pimonidazole following the manufacturer's protocol. The fluorescent images of cells in each group were observed under CLSM.

The ability of DHCaNPs to alleviate tumor hypoxia was also investigated by the changes in the expression levels of HIF-1 $\alpha$  via Western blotting analysis. In brief, the cells after different treatment were harvested and subjected to RIPA lysis buffer for 1 h. After centrifugation, the total protein concentration in the resulting solution was quantified by a BCA protein assay kit. Subsequently, the protein samples were separated by 10% sodium dodecyl-sulfate polyacrylamide gel electrophoresis (SDS-PAGE), followed by transferring onto a polyvinylidene fluoride membrane through electroblotting. The membrane was then subjected to blocking using 5% non-fat milk for a duration of 90 min at ambient temperature with agitation. This step was succeeded by an overnight incubation with the primary anti-HIF-1 $\alpha$  antibodies at 4 °C under continuous shaking. Afterward, the membrane underwent a series of washes, thrice with Tris-buffered saline with Tween (TBST), and was then incubated with the secondary antibody for an additional period of 2 h. The protein bands present on the membrane were subsequently visualized and captured employing the iBright™ FL1500 Imaging System.

## 2.9. In vivo distribution evaluation

The *in vivo* distribution of DHCaNPs was assessed by monitoring the fluorescence of ICG in a unilateral subcutaneous tumor-bearing murine model. In brief, ICG-labeled DHCaNPs were initially prepared using the aforementioned CaCO<sub>3</sub>-assisted double emulsion method, with DOX being substituted by ICG. Subsequently, the prepared nanoparticles (ICG-HCaNPs, 100  $\mu\text{l}$ ) were administered via intravenous injection into the 4T1 tumor-bearing mice. At specific time intervals, the ICG fluorescence signals in each mouse were recorded using the IVIS Lumina III System (PerkinElmer, USA). Furthermore, *ex vivo* fluorescent images of major organs (heart, liver, spleen, lung, and kidney) as well as the tumor tissue harvested at 48 h post-injection were also obtained by IVIS Lumina III System.

## 2.10. In vivo acidity and hypoxia alleviation

The *in vivo* capacity of DHCaNPs to alleviate tumor acidity was assessed employing SNARF pH indicator [35]. Briefly, 4T1 tumor-bearing mice were intravenously administered with DHCaNPs or other formulations at a DOX dosage of 5 mg/kg. After 24 h post-injection, the mice received SNARF (1 nmol per mouse) via vein injection. Twenty min later, tumor tissues were collected immediately from the euthanized mice for fluorescence imaging via IVIS Lumina III System. The pH values of tumor tissues were also calculated according to the standard protocol provided by the manufacturer.

The *in vivo* capacity of DHCaNPs to alleviate tumor hypoxia was assessed employing pimonidazole as a hypoxia probe [36]. In brief, 4T1 tumor-bearing mice were intravenously administered with DHCaNPs or other formulations at a dosage of 5 mg/kg. After 24 h post-injection, the mice received a vein injection of pimonidazole hydrochloride (0.6 mg per mouse). Tumor tissues were collected from the euthanized mice 90 min later, to prepare frozen sections for immunofluorescence staining following the protocol provided by the manufacturer. Subsequently, fluorescent images of the tumor sections were observed using a fluorescence microscope.

## 2.11. In vivo chemotherapeutic efficacy

*In vivo* chemotherapeutic efficacy of DHCaNPs was investigated using the unilateral subcutaneous tumor-bearing murine model. In brief, the 4T1 tumor-bearing mice were randomly divided into 6 groups, including PBS, free DOX, DNPs, DHNPs, DCaNPs and DHCaNPs ( $n = 5$ ). After the tumor volume reached to 60~80 mm<sup>3</sup>, the mice were intravenously injected with the aforementioned preparations at an equivalent dose of 5 mg/kg DOX on Day 0, Day 3 and Day 6, respectively. Throughout the treatment period the changes in the body weights, tumor length (L) and width (W) of each mouse were tracked every other d. The tumor volume (V) was calculated by the following formula:  $V = L \times W^2/2$ . Moreover, tumor inhibitory rate was calculated using the following formula:

$$\text{Tumor inhibitory rate(\%)} = (1 - V_T/V_C) \times 100\%$$

Where  $V_T$  represents the mean tumor volume in the treatment groups, and  $V_C$  denotes the mean tumor volume in the control group. On Day 14, the tumor tissues and major organs (heart, liver, spleen, lung and kidney) were harvested and subjected to H&E staining. Moreover, the tumor tissues were weighted, photographed and stained with TUNEL, Ki-67 for further anticancer efficacy evaluation.

### 2.12. *In vivo chemo-immunotherapy efficacy*

*In vivo* combination therapy of DHCaNP and  $\alpha$ PD-L1 was investigated using the bilateral subcutaneous tumor-bearing murine model. In brief, the tumor-bearing mice were randomly divided into 6 groups, including PBS,  $\alpha$ PD-L1, DNP+ $\alpha$ PD-L1, DHNP+ $\alpha$ PD-L1, DCaNP+ $\alpha$ PD-L1, and DHCaNP+ $\alpha$ PD-L1 ( $n = 5$ ). The primary tumor was intratumorally injected with nanoparticles at dosage of DOX 3 mg/kg on Day 0 and 3, respectively. At 24 h post injection of nanoparticles, the mice were intravenously injected with  $\alpha$ PD-L1 at a dosage of 1 mg/kg. The changes in the body weights and tumor volumes were recorded during the whole treatment period.

### 2.13. *Immunological response analysis*

To explore the mechanism of antitumor immune activation resulting from the combination treatment, another 6 groups of bilateral subcutaneous tumor-bearing mice were subjected to the same treatment as described above. At Day 2 following the second  $\alpha$ PD-L1 administration, we collected the bilateral tumor tissues and lymph nodes closed to the primary tumor. These harvested tissues were subsequently processed into a single-cell suspension using the previously established method [37]. Then, these cells were stained with corresponding fluorescently labeled antibodies for flow cytometry analysis of DCs ( $CD11c^+CD80^+CD86^+$ ) in lymph nodes,  $CD8^+$ T cells ( $CD3^+CD4^-CD8^+$ ) and Treg cells ( $CD3^+CD4^+Foxp3^+$ ) in primary and distant tumors, M1 macrophages ( $CD11b^+F4/80^+CD80^+$ ) and M2 macrophages ( $CD11b^+F4/80^+CD206^+$ ) in primary tumors. Moreover, the levels of TNF- $\alpha$  and IFN- $\gamma$  in blood serum were quantified by the corresponding ELISA kit according to the protocol provided by manufacturer.

### 2.14. *Statistical analysis*

All results are reported as the mean  $\pm$  SD. Analysis of variance (ANOVA) was employed to assess statistical significance among groups, and pairwise comparisons were conducted using Student's *t*-test. A *P* value  $< 0.05$  was considered statistically significant.

## 3. Results and discussion

### 3.1. *Preparation and characterization of DHCaNP*

In this study, the water-soluble DOX and Hb were co-encapsulated within PLGA/PLGA-PEG nanoparticles via CaCO<sub>3</sub>-assisted double emulsion method by introducing

CaCO<sub>3</sub> into their internal aqueous cavity (Fig.1A). Transmission electron microscopy (TEM) analysis revealed that the synthesized CaCO<sub>3</sub>, DOX, and Hb-loaded nanoparticles (referred to as DHCaNP) exhibited a spherical morphology with an average particle size of approximately 130 nm (Fig.1B). Furthermore, the presence of small dark dots within DHCaNP indicated the successful formulation of CaCO<sub>3</sub> nanocrystals inside the nanoparticles during the encapsulation process (Fig.1B). In contrast, Fig.1C demonstrated that the DOX and Hb dual-loaded nanoparticles without CaCO<sub>3</sub> (referred to as DHNP) did not exhibit any small dark dots inside. Dynamic light scattering (DLS) measurements revealed that the average particle size of DHCaNP was  $133.6 \pm 8.44$  nm, which was consistent with the TEM observation (Fig.1D). In addition, DHCaNP revealed a remarkably comparable size distribution profile to that of DHNP, demonstrating minimal influence from the introduction of CaCO<sub>3</sub> (Fig.1D).

The UV-Vis-NIR spectrum of DHCaNP exhibited characteristic absorption peaks at 480 nm and 405 nm, corresponding to the distinctive absorption wavelengths of DOX and Hb, respectively (Fig.1E). These prominent peaks serve as clear indicators of the successful encapsulation of both DOX and Hb within DHCaNP. As shown in Fig.1F, the EE of DOX and Hb within DHCaNP was  $64.20\% \pm 6.69\%$  and  $71.42\% \pm 8.47\%$ , respectively. In comparison, DHNP exhibited a lower efficiency in encapsulating DOX ( $42.51\% \pm 6.07\%$ ) and Hb ( $40.48\% \pm 2.22\%$ ). These results suggested that the introduction of CaCO<sub>3</sub> into the PLGA/PLGA-PEG nanoparticles led to a remarkable improvement in the EE of DOX and Hb, which could be attributed to the strong coordination interactions between the newly formed CaCO<sub>3</sub> with DOX and Hb [38]. It was also observed that DHCaNP could quickly react with proton to neutralize the acidic solution, significantly elevating its pH to a more neutral range (Fig.1G). In contrast, DHNP exhibited minimal disturbance to the pH of the acidic solution, emphasizing that the inclusion of CaCO<sub>3</sub> plays a crucial role in neutralizing the acidic tumor environment.

The investigation into the oxygen carrying ability of DHCaNP was conducted using a portable oxygen microelectrode. As demonstrated in Fig.1H, the dissolved oxygen concentration displayed a swift increase of approximately 6 mg/l within 5 min after oxygen bubbling in the solution containing free Hb. Remarkably, a comparable trend was observed in the solution containing DHCaNP, indicative of its outstanding oxygen-carrying capacity. In contrast, the solution containing CaNP exhibited only a marginal increase in oxygen concentration, implying the pivotal role of Hb incorporation within nanoparticles for efficient oxygen transportation. The drug release profile of DHCaNP against different pH was evaluated using dialysis bag method. It was found that DHCaNP exhibited a rapid drug release profile under pH 5.0, with approximately 70% of DOX released within 24 h (Fig.1I). The investigation further revealed a notable trend in the release rate of DOX from DHCaNP, which exhibited a descending order as follows: pH 5.0  $>$  pH 6.5  $>$  pH 7.4. In contrast, DHNP prepared without the incorporation of CaCO<sub>3</sub> exhibited consistent DOX release behavior when subjected to buffers with varying pH values (Fig.1I). This observation underscores the crucial

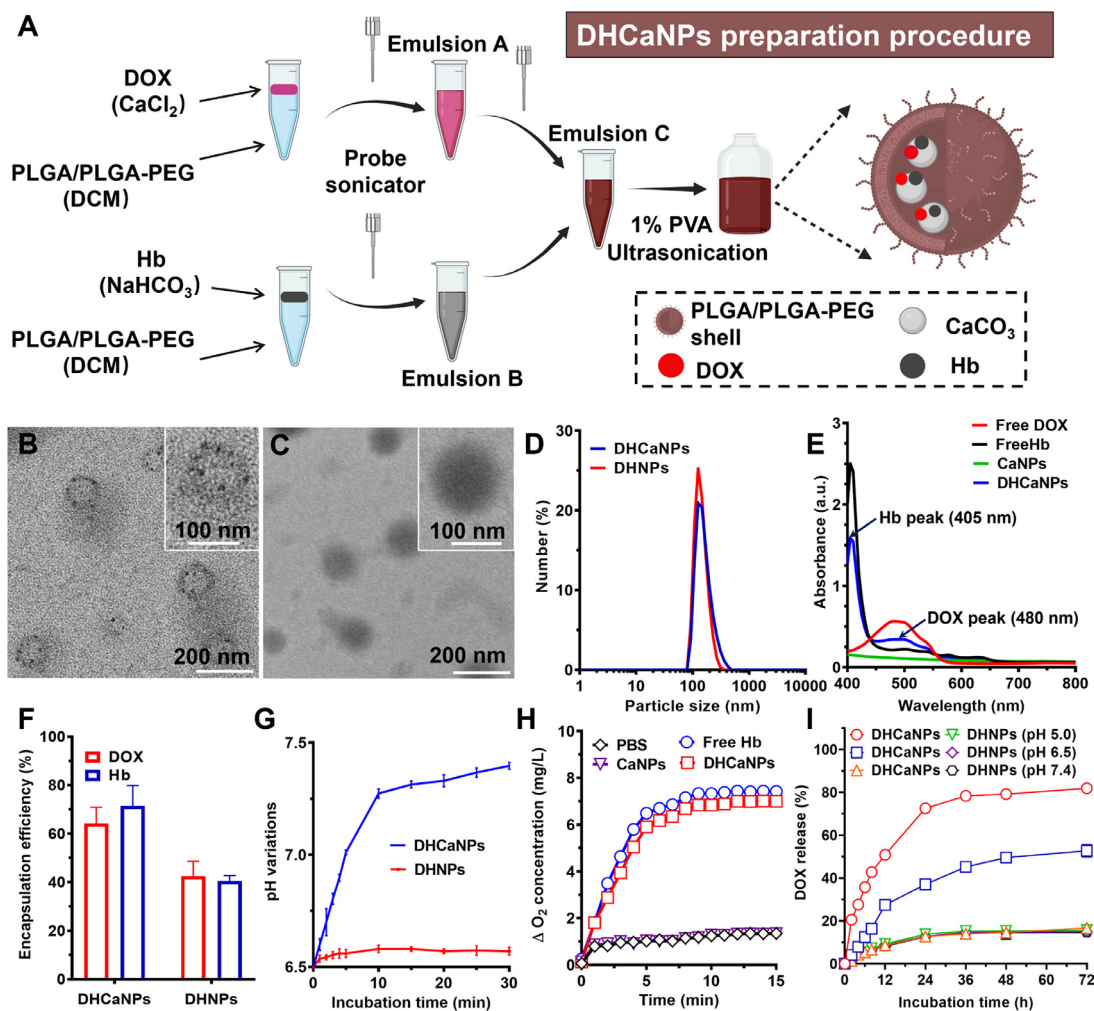


**Fig. 1** – Preparation and characterization of DHCaNPs. (A) Schematic diagram of the synthesis process of DHCaNPs; (B, C) TEM images of DHCaNPs (B) and DHNPs (C); (D) Size distribution profile of DHCaNPs and DHNPs determined by DLS; (E) UV absorption spectrum of Free DOX, Free Hb, CaNPs and DHCaNPs; (F) EE of DOX and Hb in DHCaNPs and DHNPs, respectively. (G) Changes in pH values of PBS (initial pH 6.5) following the addition of DHCaNPs or DHNPs at a final nanoparticle concentration of 2 mg/ml; (H) The measurement of oxygen levels in oxygen-free PBS after adding oxygen-saturated free Hb, CaNPs, DHCaNPs; (I) Release behavior of DOX from DHCaNPs and DHNPs under various pH values (pH=5.0, 6.0, and 7.4 at 37 °C). DHNPs refers to the nanoparticles dual-loaded with DOX and Hb, but without the inclusion of CaCO<sub>3</sub>.

role of CaCO<sub>3</sub> in imparting pH-responsive characteristics to DHCaNPs, enhancing their ability to release drugs in a controlled manner based on the environmental pH.

### 3.2. DHCaNPs reverses lactic acid-induced chemotherapy resistance

In this part, we initiated an investigation into the influence of lactic acid on the cellular internalization behaviors of DHCaNPs within 4T1 cells by employing GLSM and flow cytometry. It was observed that 4T1 cells incubated with free DOX under acidic conditions displayed a diminished fluorescence intensity in comparison to those under normal conditions (Figs. 2A, 2B and S1). This finding provided unequivocal evidence that the presence of lactic acid could markedly hinder the diffusion of DOX into cancer cells, confirming that the lactic acid has the potential to

diminish the susceptibility of cancer cells to chemotherapy. The phenomenon of chemotherapy resistance induced by lactic acid has been consistently substantiated by earlier investigations [25,26]. For DCaNPs and DHCaNPs, the fluorescence intensity of DOX within 4T1 cells was noticeably higher under acidic conditions compared to the normal conditions, displaying an intracellular internalization behavior contrary to that observed in the free DOX group in normal conditions (Figs. 2A, 2B and S1). There were possible two reasons accounting for this observation: (i) The acidic conditions accelerated the release of free DOX molecules, which had a better diffusion capability when contrasted with nanoparticles with significantly larger sizes; (ii) The inclusion of CaCO<sub>3</sub> equips DCaNPs or DHCaNPs with a remarkable capacity for neutralizing lactic acid, therefore further amplifying the intracellular uptake of DOX within cancer cells. The successful removal of lactic acid by DCaNPs

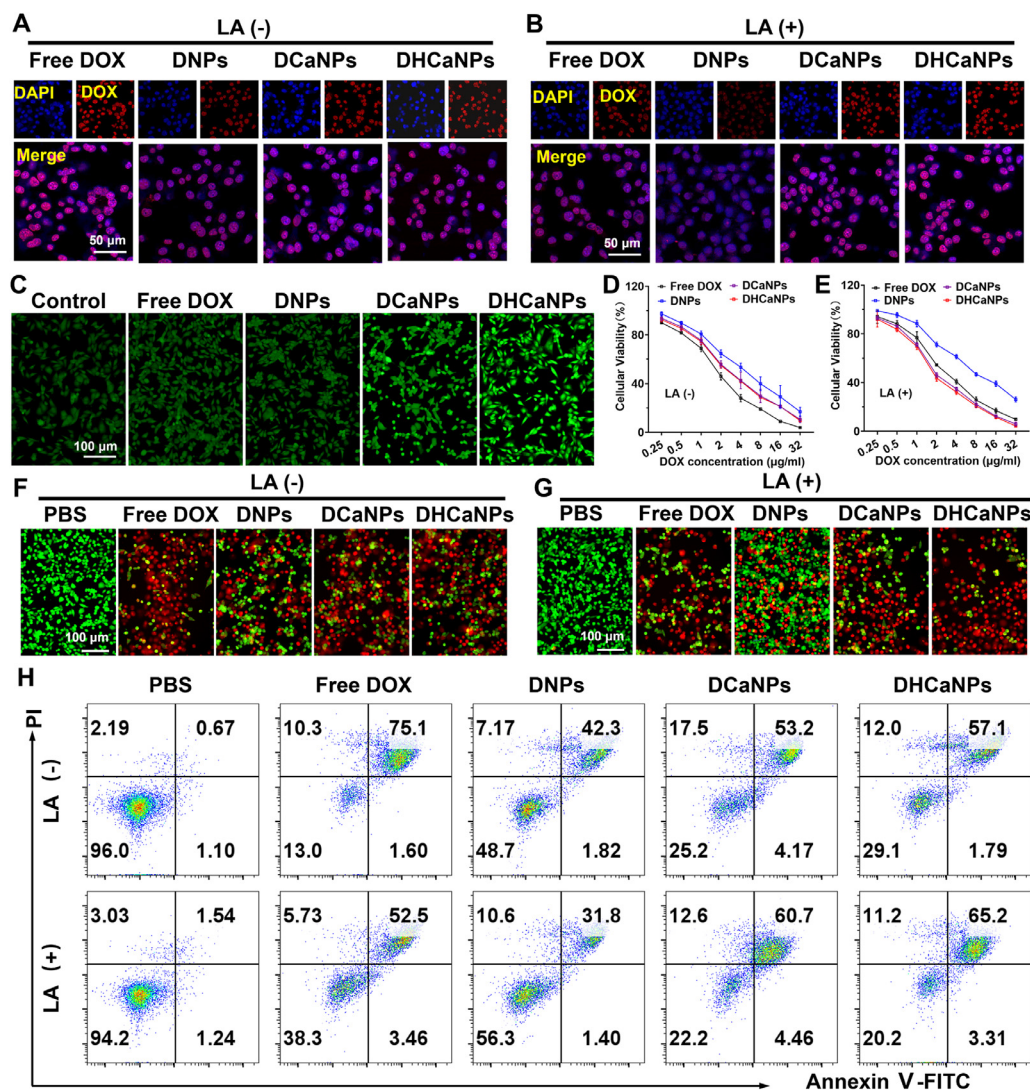


**Fig. 2 – DHCaNPs reverses lactic acid-induced chemotherapy resistance *in vitro*.** (A, B) Representative confocal images of 4T1 cells subjected to various treatments for 12 h under normal (A) and acidic (B) conditions. (C) Intracellular BCECF fluorescence intensity in 4T1 cells subjected to various treatments for 12 h under acidic condition. (D, E) Cell viability of 4T1 cells after incubation with different concentrations of free DOX, DCaNPs, DNPs or DHCaNP for 48 h under normal (D) and acidic (E) conditions. (F, G) Live-dead staining assay of 4T1 cells subjected to various treatments for 48 h under normal (F) and acidic (G) conditions. (H) Annexin V-FITC/PI apoptosis assay of 4T1 cells subjected to various treatments for 48 h under normal and acidic conditions. It should be noted that the Hb-loaded nanoparticles were saturated with oxygen before performing cellular study.

and DHCaNPs was confirmed by measuring the pH values of culture medium and the change in the intracellular fluorescence intensity using a pH detection probe (Figs. 2C and S2). Moreover, in the absence of lactic acid, we found that the 4T1 cells treated with DCaNPs and DHCaNPs displayed significantly enhanced DOX fluorescence signals compared to those subjected to DNPs (Figs. 2A, 2B and S1). This result could be attributed to that the faster release of DOX from the CaCO<sub>3</sub>-incorporated nanoparticles upon intracellular internalization [38].

Subsequently, *in vitro* anticancer efficacy of DHCaNPs on 4T1 cells was evaluated by using MTT assay. As shown in Fig. 2D and 2E, all of the examined formulations exhibited

a dose-dependent cytotoxicity, wherein an increased DOX dosage led to an enhanced cell-killing efficacy. According to MTT results, the half-maximal inhibitory concentration (IC<sub>50</sub>) of free DOX, DNPs, DCaNPs and DHCaNPs against 4T1 cells in normal conditions were measured to be  $1.87 \pm 0.15$ ,  $4.97 \pm 0.13$ ,  $3.11 \pm 0.29$  and  $2.96 \pm 0.12$  µg/ml, respectively. In contrast, the IC<sub>50</sub> values of free DOX, DNPs, DCaNPs and DHCaNPs against 4T1 cells in acidic conditions were calculated to be  $2.85 \pm 0.04$ ,  $7.90 \pm 0.25$ ,  $2.19 \pm 0.01$  and  $1.97 \pm 0.06$  µg/ml, respectively. This outcome demonstrated that the presence of lactic acid could significantly diminish the therapeutic efficacy of free DOX and DNPs, but considerably enhancing the anticancer potential

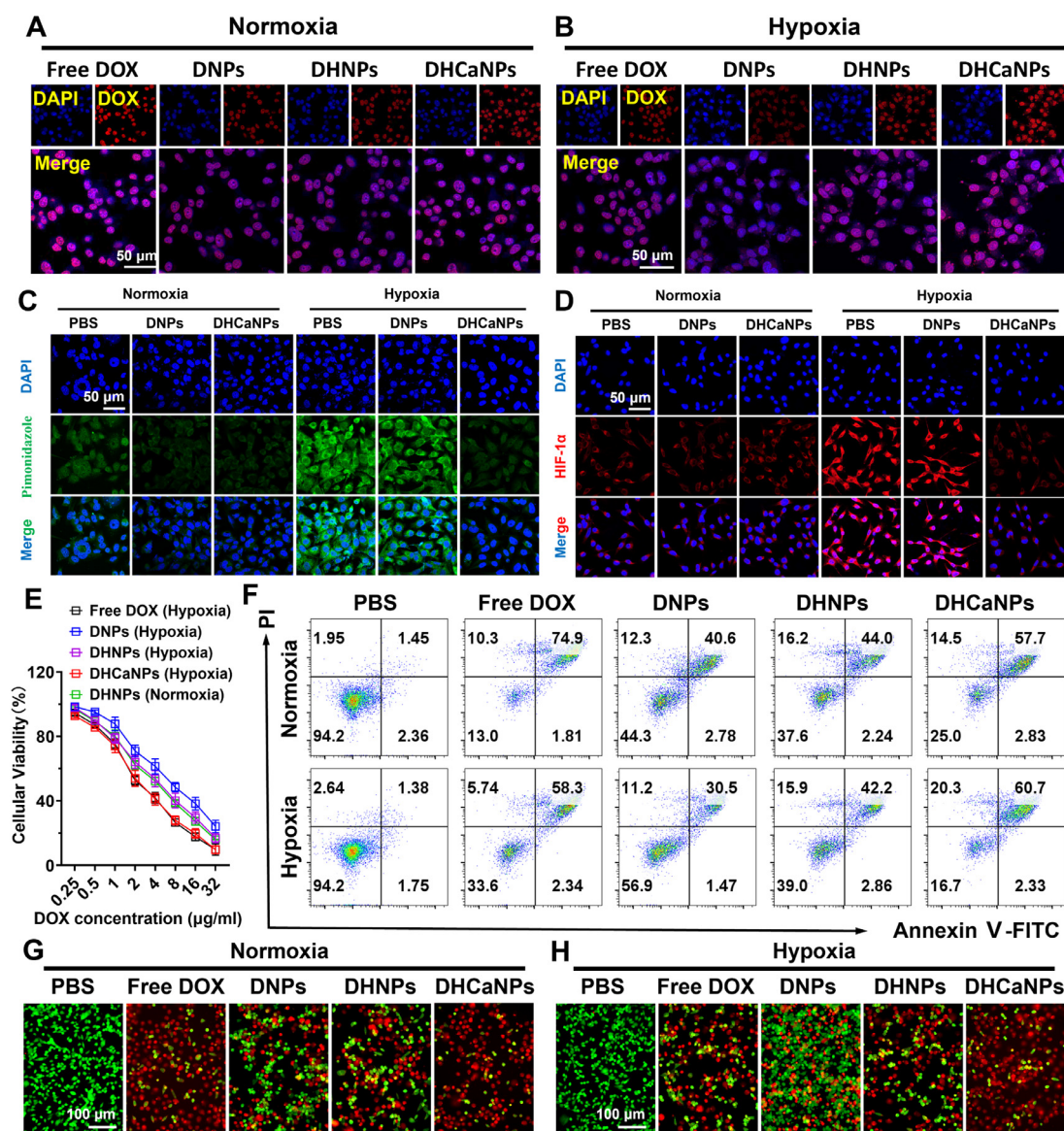


**Fig. 3 – DHCaNPs reverses hypoxia-induced chemotherapy resistance in vitro.** (A, B) Representative confocal images of 4T1 cells after undergoing various treatments for 12 h under normoxic (A) and hypoxic (B) conditions. (C, D) Immunofluorescence staining of 4T1 cells subjected to various treatments for 12 h as indicated and stained with anti-Pimonidazole (C) and anti-HIF-1 $\alpha$  (D) primary antibodies. (E) Cell viability of 4T1 cells subjected to various preparations with DOX concentrations ranging from 0 to 32  $\mu\text{g/ml}$  over 48 h. (F) Annexin V-FITC/PI apoptosis assay of 4T1 cells subjected to various treatments for 48 h under normoxic and hypoxic conditions. (G, H) Live-dead staining assay of 4T1 cells subjected to various treatments for 48 h under normoxic (G) and hypoxic (H) conditions. It should be noted that the Hb-loaded nanoparticles were saturated with oxygen before performing cellular study.

of DCaNPs and DHCaNPs. The reversal of lactic acid-induced chemotherapy resistance by DCaNPs and DHCaNPs was further substantiated via cell apoptosis assay. As depicted in Fig. 2H, the apoptotic rates of cells subjected to treatment with DCaNPs and DHCaNPs under acidic conditions were 60.7% and 65.2%, respectively. These rates were comparable to those of cells treated with free DOX under normal condition, yet notably exceeded the rates observed in the other experimental groups. This discovery suggests that incorporating CaCO<sub>3</sub> into DOX-loaded nanoparticles significantly augments their capacity to trigger cell apoptosis in acidic environments. The live-dead cell assay further confirmed the amplified

anticancer efficacy of DCaNPs and DHCaNPs under acidic conditions, revealing a greater number of dead cells compared to the other treatment groups (Fig. 2F and 2G). Taken together, these results demonstrate that DHCaNPs is capable of overcoming the chemotherapy resistance induced by lactic acid.

### 3.3. DHCaNPs reverses hypoxia-induced chemotherapy resistance

In this section, we embarked on an inquiry into the impact of hypoxia on the intracellular uptake patterns of

DHCaNPs within 4T1 cells via CLSM and flow cytometry. As shown in Figs. 3A, 3B and S3, both free DOX and DNPs displayed a reduced cellular internalization in hypoxic condition, as evidenced by the diminished DOX fluorescence intensity. Conversely, the hypoxic cells treated with DHNPs and DHCaNPs exhibited fluorescence intensities similar to those of normal cells, which was significantly stronger than the hypoxic cells treated with DNPs. This result illustrated that the inclusion of Hb could enhance the cellular uptake capacity of the nanomedicine in a hypoxic environment, which was due to Hb-mediated hypoxia alleviation. The superior ability of DHCaNPs to attenuate hypoxia was firstly confirmed by using pimonidazole as a hypoxia probe. As depicted in Fig.3C, notably intense pimonidazole fluorescence signals were detected in 4T1 cells cultured in hypoxia, whether exposed to PBS or DNPs. These signals indicate the pronounced hypoxia levels within the cells. In contrast, we observed that the hypoxic cells treated with DHCaNPs exhibited pimonidazole fluorescence intensity comparable to that of normal cells in the treatment groups, indicating a significant reduction in cellular hypoxia levels induced by DHCaNPs. Furthermore, we also compared the expression levels of HIF-1 $\alpha$  in different groups, as it serves as an intrinsic marker employed in clinical settings to assess tissue hypoxia [39]. Western blotting and immunohistochemistry analyses indicated a significant upregulation of HIF-1 $\alpha$  levels under hypoxic conditions (Figs. 3D and S4). The treatment of DHCaNPs could largely decrease the expression level of HIF-1 $\alpha$  within hypoxic cells. However, it's noteworthy that the expression level of HIF-1 $\alpha$  remained high in DNPs-treated hypoxic cells, attributable to the absence of oxygen-carrying capacity in DNPs. These findings validate that DHCaNPs could effectively supply oxygen to tumor cells and alleviate tumor hypoxia.

Subsequently, *in vitro* therapeutic efficacy of DHCaNPs on hypoxic cells was evaluated. MTT results suggested that DHCaNPs exhibited a dose-dependent cytotoxicity towards the hypoxic cells (Fig.3E). The IC<sub>50</sub> values of free DOX and DNPs under hypoxic condition was calculated to be  $2.84 \pm 0.30$  and  $7.89 \pm 0.78$ , respectively. This result suggests that the cytotoxicity of free DOX and DNPs against cancer cells could be significantly compromised under hypoxic conditions, in line with prior research findings [33]. Conversely, the calculated IC<sub>50</sub> values for DHNPs and DHCaNPs against hypoxic cells were  $4.98 \pm 0.77$  and  $2.85 \pm 0.22$ , respectively, and these values were comparable to those observed under normoxic conditions. The reversal of hypoxia-induced chemotherapy resistance by Hb-loaded nanoparticles (DHNPs and DHCaNPs) was further substantiated through cell apoptosis and live-dead assay (Fig.3F-3H). Overall, these findings suggest that DHCaNPs significantly improved therapeutic efficacy of DOX in combating hypoxic breast cancer cells.

### 3.4. Biodistribution and modulation potency of DHCaNPs

*In vivo* distribution of DHCaNPs was evaluated by tracking the fluorescence of ICG in a 4T1 tumor-bearing murine model. ICG is well-known for its excellent near-infrared fluorescence properties, frequently serving as a fluorescent alternative to

DOX in real-time imaging applications [40,41]. The ICG-labeled nanoparticle (abbreviated as ICG-HCaNPs) was prepared using the same protocol described above. After the 4T1 tumor-bearing mice were intravenously administrated with ICG-HCaNPs, a gradual increase of fluorescence signals within the tumor regions was observed via an *in vivo* imaging system (Fig.4A). Semiquantitative data revealed that the tumor sites exhibited a gradually enhanced ICG fluorescence during the initial 24 h post-injection, followed by a plateau in the subsequent 24 h (Fig.4A and 4C). In comparison, the 4T1 tumor-bearing mice treated with free ICG showed a quick decrease of ICG fluorescence in the tumor sites after 2 h post-injection (Fig.4A and 4C). These findings emphasized the effective targeting and accumulation of DHCaNPs in the tumor sites. Then, *ex vivo* fluorescent images of the tumor tissue and major organs harvested at 48 h post-injection were captured to further confirm the superior tumor-homing ability of DHCaNPs. It was observed that the fluorescence intensity of tumors in ICG-HCaNPs groups in much higher than that of the free ICG group, further indicating the excellent tumor targeting and retention abilities of DHCaNPs (Fig.4B and 4D). In addition, noticeable fluorescence signals were observed in the liver tissues from the ICG-HCaNPs groups, which was a common phenomenon associated with the uptake of nanoparticles by the reticuloendothelial system [42,43].

The potency of DHCaNPs in neutralizing tumor acidity was carefully investigated by using SNARF-1 as the tumor pH detection probe. It was found that the tumors harvested from DCaNPs, HCaNPs, and DHCaNPs groups exhibited a notable reduction in the ratio of SNARF-1 fluorescence intensities excited at 580 nm and 640 nm, in contrast to both the control and DHNPs groups (Fig.4E). In addition, the pH values of tumors were measured to be  $6.96 \pm 0.05$ ,  $6.95 \pm 0.01$  and  $7.05 \pm 0.11$  after treated with DCaNPs, HCaNPs, and DHCaNPs, respectively (Fig.4F). In contrast, the pH values of tumors collected from DHNPs was measured to be  $6.61 \pm 0.05$ , which was similar to that of control groups ( $6.55 \pm 0.10$ ). These findings demonstrated that the incorporation of CaCO<sub>3</sub> could equip the nanoparticles with a remarkable ability to neutralize tumor acidity. Subsequently, we assessed the potential of DHCaNPs to alleviate tumor hypoxia using pimonidazole as the probe for detecting hypoxic conditions within the tumor microenvironment. As depicted in Fig.4G, the pimonidazole-specific fluorescence signals observed in tumor tissues from the DHNPs, HCaNPs, and DHCaNPs groups exhibited considerably lower intensity compared to those from the control and DCaNPs groups. This pronounced contrast indicates the successful oxygen delivery to the tumor region through the utilization of Hb-loaded nanoparticles. Overall, these results conclusively demonstrated that DHCaNPs effectively neutralize tumor acidity and concurrently attenuate tumor hypoxia.

### 3.5. DHCaNPs can potentiate chemotherapy

The potential of DHCaNPs in enhancing the therapeutic outcome of chemotherapy was investigated using orthotopic 4T1 tumor-bearing murine models (Fig.5A). The tumor-bearing mice received the following treatments: (1) PBS, (2)

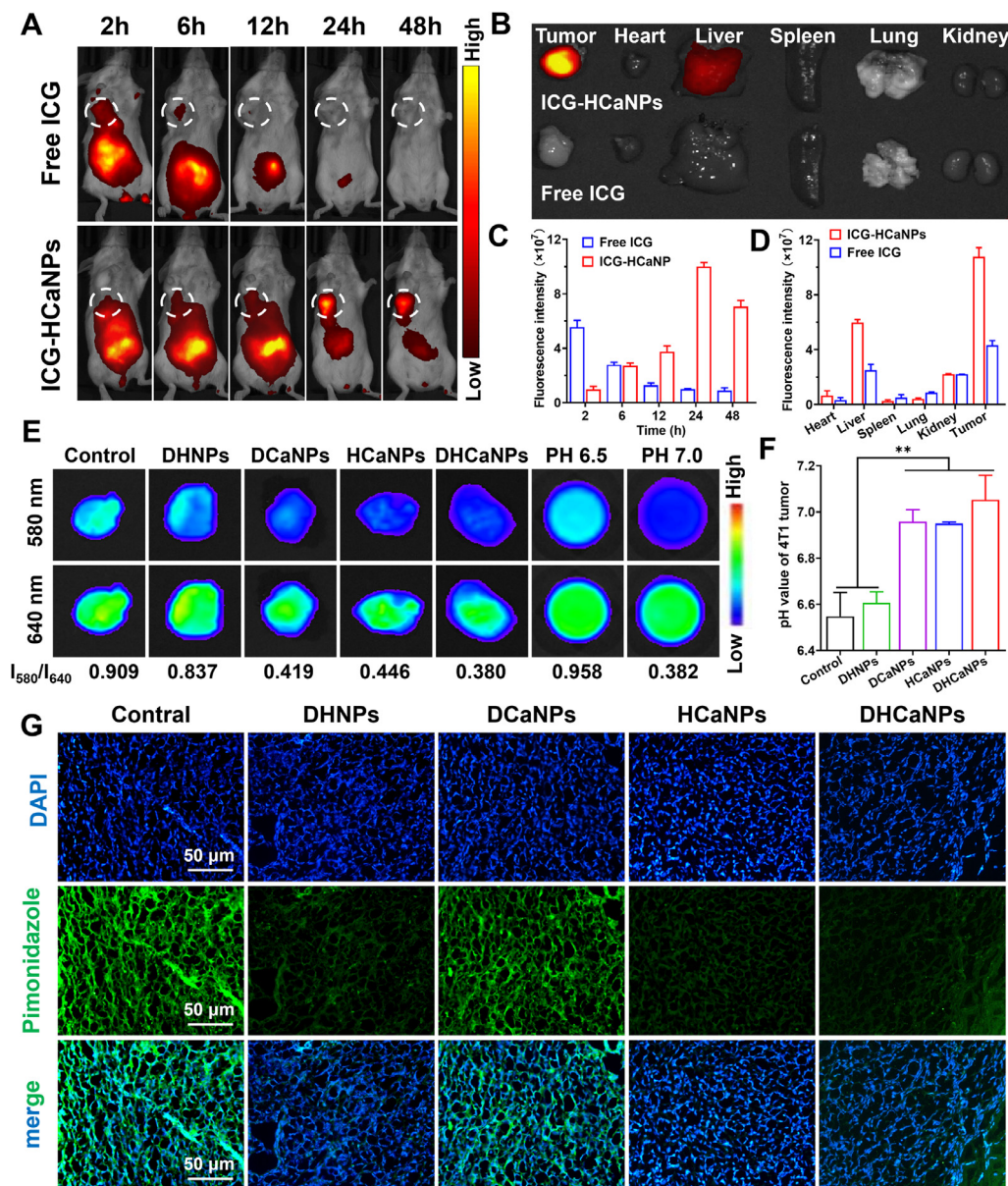


**Fig. 4 – Biodistribution and modulation potency of DHCaNs in vivo.** (A) *In vivo* fluorescence imaging of 4T1 tumor-bearing mice intravenously injected with ICG-HCaNs or free ICG by recording ICG fluorescence within excitation and emission in the NIR I region (700–900 nm). (B) *Ex vivo* fluorescence image of tumor and major organs harvested at 48 h post intravenous injection. (C) Time-dependent MFI analysis of ICG fluorescence from ICG-HNPs and free ICG at the tumor site post intravenous injection. (D) The corresponding MFI values (ICG fluorescence) of tumor and major organs harvested at 48 h post-injection. (E) Representative fluorescence images of tumor tissues harvested 24 h post various treatments. The mice were intravenously injected with a pH-sensitive dye (SNARF-4F) 20 min prior to sacrifice. (F) The pH values of tumor tissues harvested 24 h post various treatments. The pH is measured as the ratio of two peaks in the SNARF emission at 580 nm and 640 nm, converting the ratio into pH using a calibration curve. (G) Representative confocal images of tumor tissues harvested 24 h post various treatments. The mice were intravenously injected with pimonidazole 1.5 h prior to sacrifice. It should be noted that the Hb-loaded nanoparticles were saturated with oxygen before performing animal experiment. \* $P < 0.05$ , \*\* $P < 0.01$ , \*\*\* $P < 0.001$ , \*\*\*\* $P < 0.0001$ .

free DOX, (3) DNPs, (4) DHNPs, (5) DCaNs and (6) DHCaNs. It was observed that the tumor-bearing mice treated with DOX-loaded nanoparticles (DNPs, DHNPs, DCaNs, and DHCaNs) demonstrated a slower rate of increase in tumor volumes compared to both the free DOX and negative PBS groups

(Fig.5B and 5C). This result suggested that the application of nano-scale delivery systems could largely enhance the chemotherapeutic efficacy against tumor growth, which was possibly due to their tumor-targeting ability via the enhanced permeability and retention (EPR) effect [44]. In addition, we

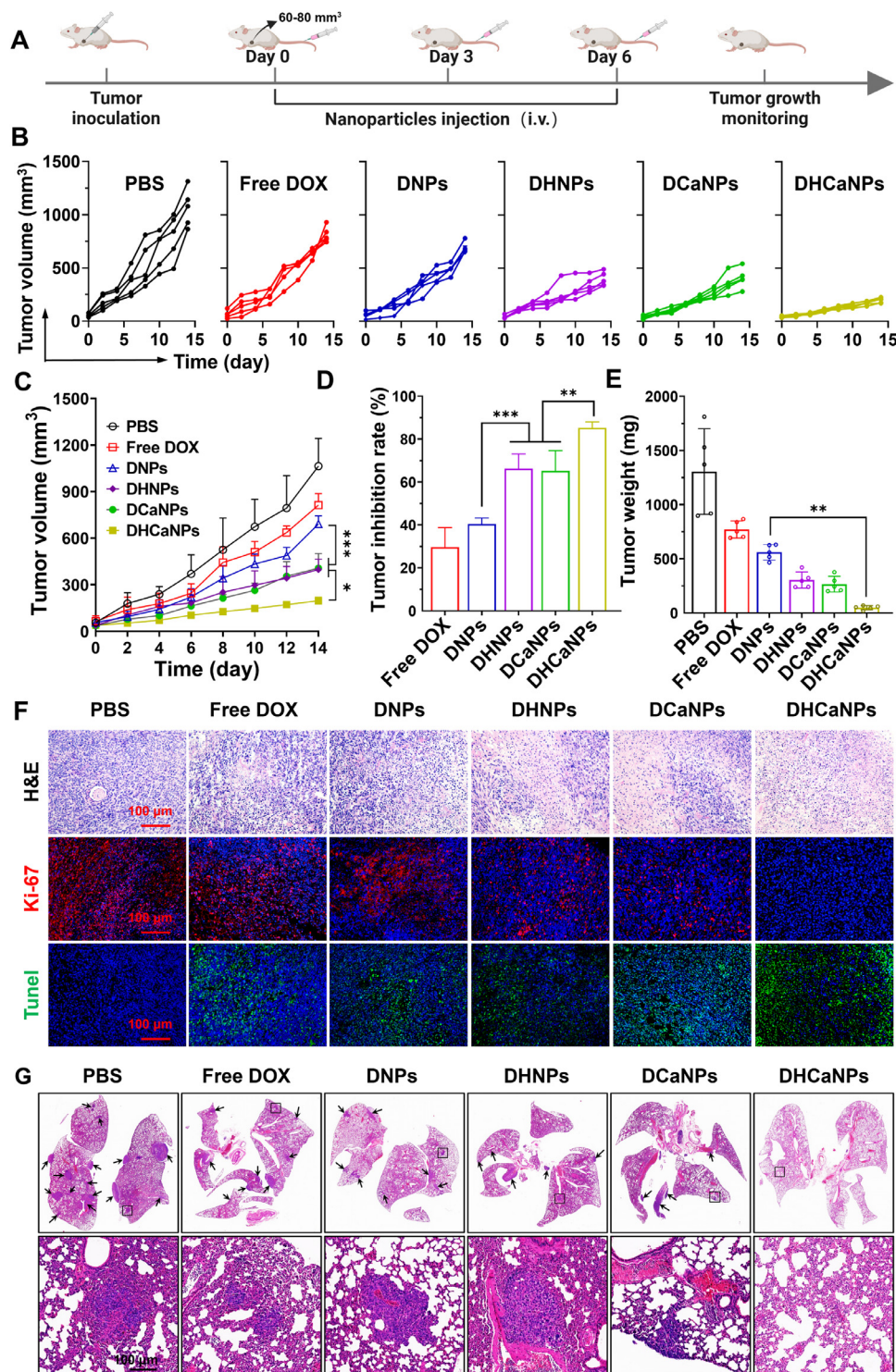


**Fig. 5 – In vivo chemotherapy efficiency of DHCaNPs. (A)** Schematic depiction of experimental procedure. **(B, C)** The changes in individual tumor volume **(B)** and average tumor volume **(C)** of 4T1 tumor-bearing mice subjected to various treatments ( $n = 5$ ). **(D)** The tumor inhibition rate of DHCaNPs and other preparations. **(E)** The average weight of tumor tissue harvested at 14-d post different treatments. **(F)** H&E, Ki-67 (red) and Tunnell (green) staining analysis of tumor slices obtained at 14-d post different treatments. **(G)** H&E staining and local enlarged images of lung metastasis at 14-d post different treatments. It should be noted that the Hb-loaded nanoparticles were saturated with oxygen before performing animal experiment. \* $P < 0.05$ , \*\* $P < 0.01$ , \*\*\* $P < 0.001$ , \*\*\*\* $P < 0.0001$ .

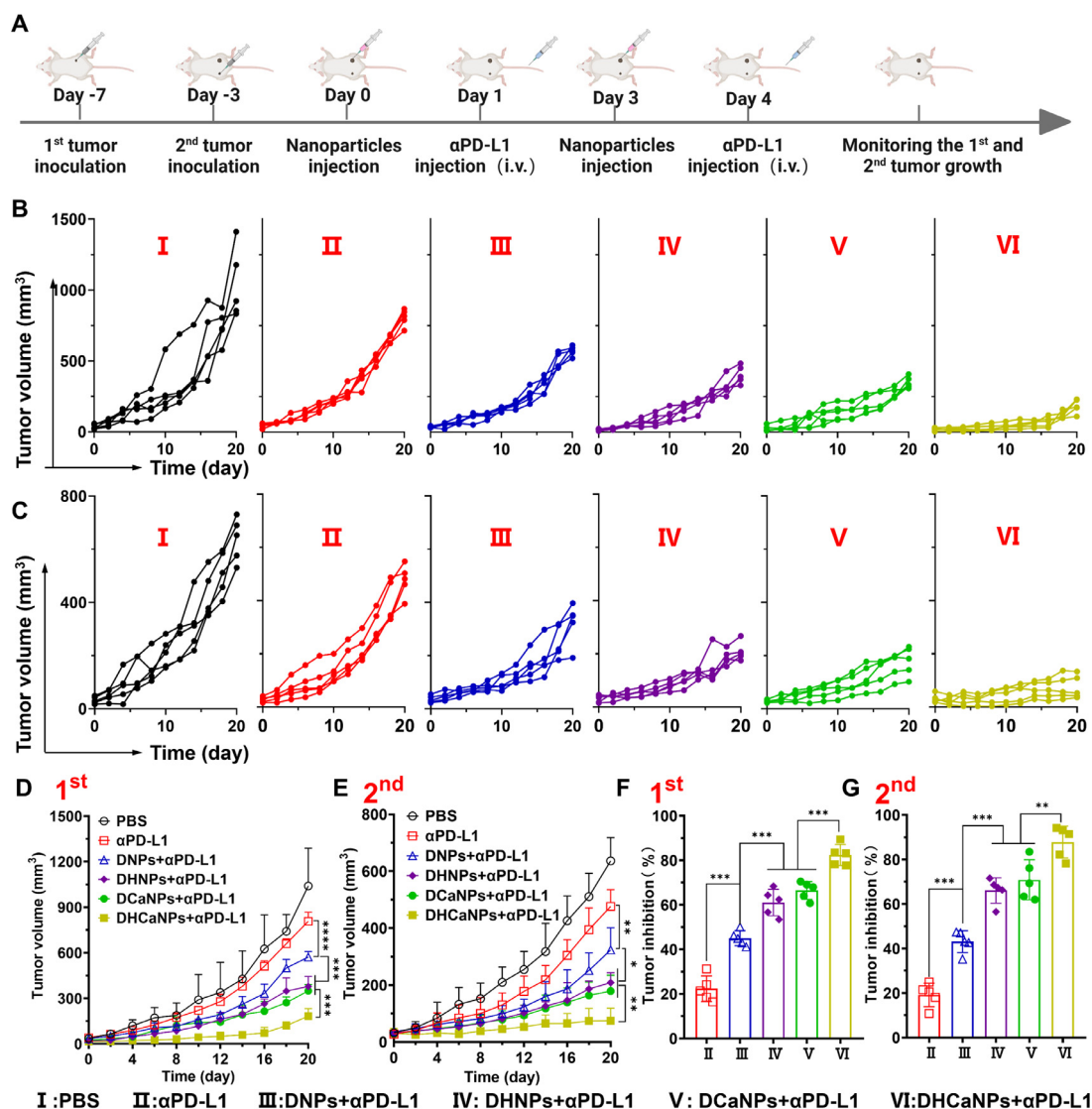


**Fig. 6 – In vivo chemo-immunotherapy efficacy of DHCaNPs with  $\alpha$ PD-L1. (A) Schematic illustration of chemo-immunotherapy treatment protocols. (B, C) Tumor growth curves of primary tumors (B) and distant tumors (C) after various treatments. (D, E) The tumor inhibition rates of DHCaNPs and other preparations against primary tumors (D) and distant tumors (E). (F, G) The individual tumor growth curves of primary tumors (F) and distant tumors (G) after various treatments ( $n = 5$ ). It should be noted that the Hb-loaded nanoparticles were saturated with oxygen before performing animal experiment. \* $P < 0.05$ , \*\* $P < 0.01$ , \*\*\* $P < 0.001$ , \*\*\*\* $P < 0.0001$ . I, II, III, IV, V and VI represents PBS,  $\alpha$ PD-L1, DNPs+ $\alpha$ PD-L1, DHNPs+ $\alpha$ PD-L1, DCaNPs+ $\alpha$ PD-L1, and DHCaNPs+ $\alpha$ PD-L1, respectively.**

also noticed that DHNPs and DCaNPs were more effective at reducing tumor growth rate than DNPs, which suggested that the inclusion of Hb or  $\text{CaCO}_3$  could endow the DOX-loaded nanoparticle with an enhanced anticancer ability (Fig.5B and 5C). It's noteworthy that within the entire spectrum of groups, DHCaNPs showcased the most formidable capacity for inhibiting tumor growth. This phenomenon underscored the synergistic enhancement of chemotherapeutic efficacy resulting from the dual encapsulation of Hb and  $\text{CaCO}_3$ . The tumor inhibitory rate of DHCaNPs was calculated to be  $85.23\% \pm 2.80\%$  by using a previously published method [45], which was much higher than the other treatment groups (Fig.5D). The superior anticancer ability of DHCaNPs

was further substantiated through visual documentation and precise weighing of the tumors collected at 14 d post-injection (Figs. 5E and S5A).

The excellent anticancer ability of DHCaNPs was also studied by H&E, TUNEL and Ki-67 staining of the tumor tissues harvested at Day 14. As shown in Fig.5F, it was found that the mice received DHCaNPs treatment exhibited distinct signs of tumor cell apoptosis with discernible chromatin condensation and cellular shrinkage as evidenced by H&E staining. Moreover, there was minimal evidence of tumor cell proliferation, represented by the red coloration in Ki-67 staining, and notably, the highest count of apoptotic cells, identifiable by the green coloration in TUNEL sections

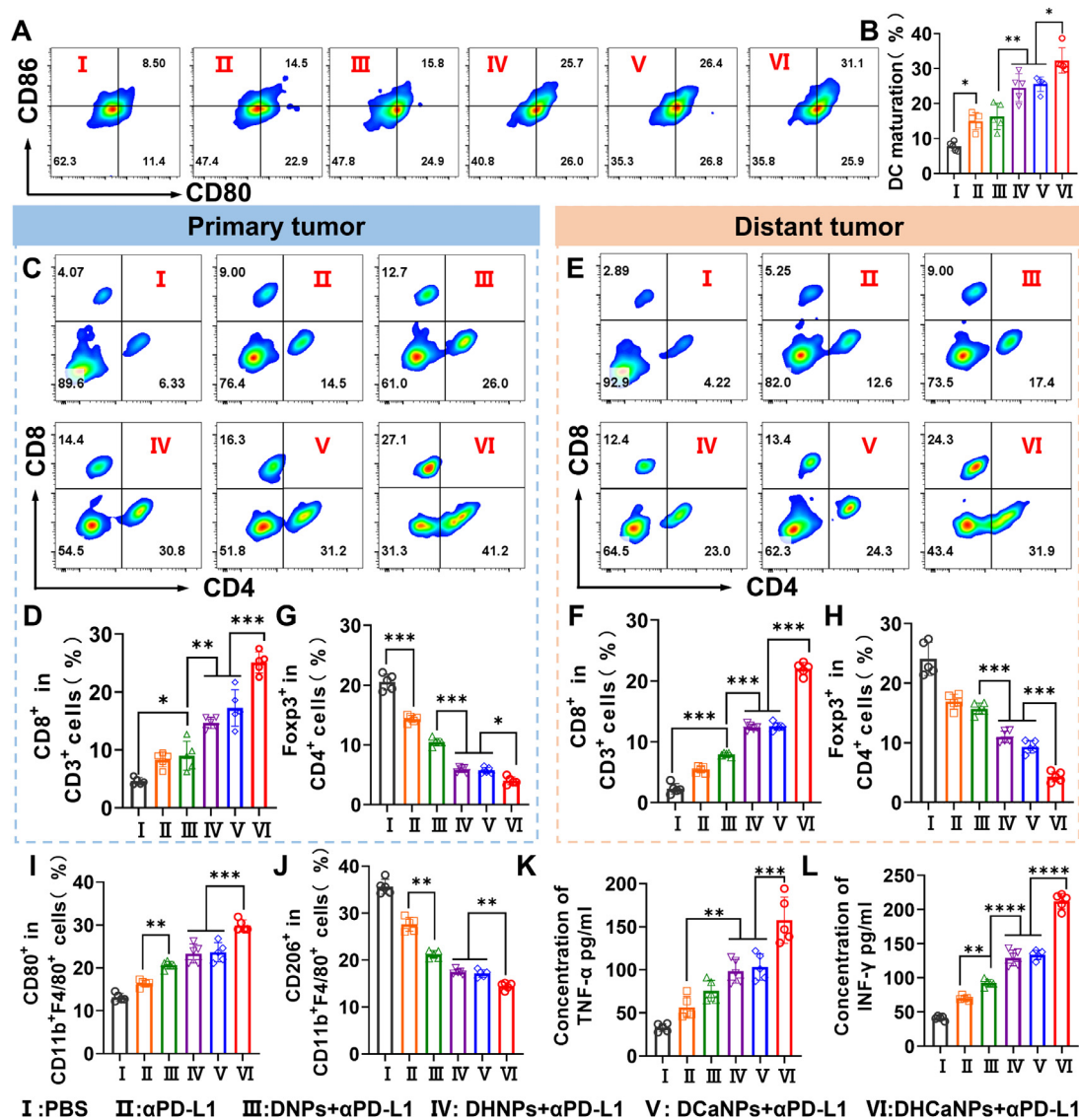


**Fig. 7** – Immune evaluation of the bilateral tumor models after different treatments. Representative flow cytometric contour plots (A) and corresponding semiquantitative analysis (B) of the matured (CD11c<sup>+</sup>CD80<sup>+</sup>CD86<sup>+</sup>) in lymph nodes adjacent to the primary tumor in mice with various treatments; Representative flow cytometric contour plots (C) and corresponding semiquantitative analysis (D) of CD3<sup>+</sup>CD4<sup>-</sup>CD8<sup>+</sup> T cells in primary tumors after various treatments; Representative flow cytometric contour plots (E) and corresponding semiquantitative analysis (F) of CD3<sup>+</sup>CD4<sup>-</sup>CD8<sup>+</sup> T cells in distant tumors after various treatments; Quantitative analysis of Treg cells (CD3<sup>+</sup>CD4<sup>+</sup>Foxp3<sup>+</sup>) in primary tumors (G) and distant tumors (H) after various treatments; Quantitative analysis of M1 macrophage (CD11b<sup>+</sup>F4/80<sup>+</sup>CD80<sup>+</sup>) percentage (I) and M2 phenotype macrophage (CD11b<sup>+</sup>F4/80<sup>+</sup>CD206<sup>+</sup>) percentage (J) in primary tumors after various treatments. (K) The serum TNF- $\alpha$  levels after various treatments. (L) The serum IFN- $\gamma$  levels after various treatments. It should be noted that the Hb-loaded nanoparticles were saturated with oxygen before performing animal experiment ( $n = 5$ ). \* $P < 0.05$ , \*\* $P < 0.01$ , \*\*\* $P < 0.001$ , \*\*\*\* $P < 0.0001$ . I, II, III, IV, V and VI represents PBS,  $\alpha$ PD-L1, DNP+ $\alpha$ PD-L1, DHNP+ $\alpha$ PD-L1, DCaNP+ $\alpha$ PD-L1, and DHCaNP+ $\alpha$ PD-L1, respectively.

(Fig.5F). These findings further confirmed the superior tumor suppression ability of DHCaNPs. Upon close examination of the H&E staining of lung tissues, we observed that numerous metastatic foci were present in the lung tissues obtained from the PBS and free DOX groups (Fig.5G). The administration of DNPs, DHNPs, and DCaNPs could effectively reduce metastatic area, but complete prevention of lung metastasis remains

challenging. Strikingly, the DHCaNPs-treated group exhibited an absence of observable metastatic foci, which suggested that DHCaNPs had a strongest ability to inhibit tumor metastasis (Fig.5G). Taken together, these findings implied that DHCaNPs could effectively potentiate chemotherapy by simultaneously neutralizing tumor acidity and attenuating tumor hypoxia.

The biocompatibility of DHCaNPs was investigated by monitoring the body weight change and the histological examinations of major organs (heart, liver, spleen, and kidney) using H&E staining. It was revealed that the administration of DHCaNPs had a minimal impact on the fluctuations in body weights of the mice during the entire course of treatment (Fig. S5B). Furthermore, our findings indicated that the administration of DHCaNPs did not result in noticeable disturbance to the major organs, as evidenced by histological examinations (Fig. S6). Collectively, the aforementioned results underscore the biocompatibility of DHCaNPs at the evaluated dosage, suggesting their suitability as a biocompatible agent.

### 3.6. DHCaNPs can boost chemo-immunotherapy

The therapeutic efficacy of combining DHCaNPs with  $\alpha$ PD-L1 immunotherapy against breast cancer was carefully investigated utilizing models of primary and metastatic tumor-bearing mice (Fig. 6A). By recording the tumor sizes, it was found that the  $\alpha$ PD-L1 monotherapy exhibited challenges in halting the progression of both primary and distant tumors (Fig. 6B-6E). As anticipated, the mice subjected to the combined treatment of DNP and  $\alpha$ PD-L1 exhibited a moderate inhibitory effect on both the primary and distant tumors. However, the ability of DNP+ $\alpha$ PD-L1 to inhibit bilateral tumor growth was less pronounced compared to the DHCaNPs+ $\alpha$ PD-L1 and DCaNPs+ $\alpha$ PD-L1 groups (Fig. 6B-6E). In addition, the tumor inhibitory rate of DHCaNPs plus  $\alpha$ PD-L1 against primary and distant tumors was calculated to be  $82.42\% \pm 4.76\%$  and  $87.82\% \pm 7.15\%$ , which was much higher than the other treatment groups (Fig. 6F and 6G). These findings revealed that the combination treatment of DHCaNPs with  $\alpha$ PD-L1 are more efficient in inhibiting the growth of both primary and distant tumors. It has been documented that the act of attenuating tumor acidity and hypoxia could substantially alleviate tumor immunosuppression, consequently bolstering a diverse range of cancer treatments including immunotherapy [46,47]. Furthermore, the combination therapy of DHCaNPs and  $\alpha$ PD-L1 demonstrated the highest efficacy in suppressing the growth of both primary and distant tumors as compared with the other treatment groups, which could be attributed to the dual capacity of DHCaNPs to attenuate tumor acidity and hypoxia, therefore largely amplifying the anticancer efficacy of chemo-immunotherapy. Moreover, these treatments had a marginal impact on the body weights of the treated mice (Fig. S7).

Subsequently, the antitumor immune response triggered by DHCaNPs was assessed through the analysis of single-cell suspensions obtained from bilateral tumors or lymph nodes near the primary tumor in mice subjected to different treatments, using flow cytometry. It was observed that the combination treatment of DHCaNPs and  $\alpha$ PD-L1 demonstrated a significant enhancement in DCs maturation within the lymph nodes adjacent to the primary tumors ( $P < 0.0001$ ). This enhancement surpassed that of other groups, including those subjected to  $\alpha$ PD-L1 alone, DNP+ $\alpha$ PD-L1, DCaNPs+ $\alpha$ PD-L1, and DHCaNPs+ $\alpha$ PD-L1 (Fig. 7A and 7B). These

results indicate that DHCaNPs plus  $\alpha$ PD-L1 treatment largely promotes the facilitation of DCs maturation. Additionally, the DHCaNPs combined with  $\alpha$ PD-L1 treatment led to an increased intratumoral infiltration of CD8<sup>+</sup> T cells, evident in both primary tumors and distant tumors (Fig. 7C-7F). We also found that the combination therapy of DHCaNPs and  $\alpha$ PD-L1 exhibited a remarkable capacity to significantly restrict the intratumoral frequency of regulatory T cells (Tregs) in bilateral tumors ( $P < 0.0001$ ), surpassing the effectiveness of other treatment groups (Figs. 7G-7H and S8A-S8B). Besides, there was a remarkable increase in the percentages of pro-inflammatory M1 phenotype tumor-associated macrophages (TAMs) but a dramatic reduction of anti-inflammatory M2 phenotype TAMs in the primary tumors (Figs. 7I-7J and S9A-S9B), collectively highlighting a distinct shift in TAM polarization from M2 to M1 phenotype as a result of the DHCaNPs combined with  $\alpha$ PD-L1 treatment. Moreover, the treatment of DHCaNPs plus  $\alpha$ PD-L1 were more effective in increasing the serum levels of cytotoxic TNF- $\alpha$  and IFN- $\gamma$  in the tumor-bearing mice (Fig. 7K and 7L). This result also suggested that DHCaNPs plus  $\alpha$ PD-L1 treatment could remarkably trigger systemic immune responses. Overall, these findings provided compelling evidence that such DHCaNPs plus  $\alpha$ PD-L1 treatment had a superior capability of triggering robust systemic immune responses, which was accomplished through the reversal of the immunosuppressive TME, the facilitation of DCs maturation, as well as the promotion of CD8<sup>+</sup> T cell infiltration, therefore largely enhancing the chemo-immunotherapy against TNBC.

## 4. Conclusions

In this study, we developed a pH-responsive nanoplateform dual-loaded with DOX and Hb via a CaCO<sub>3</sub>-assisted emulsion method, aiming for enhanced treatment of TNBC. The prepared DHCaNPs exhibited a greater capacity for encapsulating both DOX and Hb in comparison to their counterparts lacking CaCO<sub>3</sub>. Moreover, DHCaNPs displayed a pH-dependent drug release profile, which holds promising prospects for cancer treatment. Owing to the presence of CaCO<sub>3</sub> and Hb, DHCaNPs exhibited an exceptional ability to concurrently alleviate tumor acidity and hypoxia, significantly enhancing the therapeutic efficacy of chemotherapy against TNBC. In addition, DHCaNPs could effectively trigger systemic antitumor immune responses by increasing the frequency of tumor-infiltrating effector lymphocytes and reducing the frequency of various immunosuppressive cells. As a result, DHCaNPs could synergize with  $\alpha$ PD-L1 immunotherapy to effectively suppress the growth of both primary and metastatic TNBC. In summary, our study reveals that DHCaNPs with dual capacity of attenuating tumor acidic and hypoxia could largely enhance chemo-immunotherapy in combating TNBC. However, further studies, including optimization of large-scale production techniques and clinical evaluations, is requisite prior to the clinical application of this promising nanoplateform.

## Conflict of interest

The authors declare no conflict of interest.

## Acknowledgments

This work was supported by the Key R&D Program of Lishui City (2021ZDYF12, 2022ZDYF07, 2023zdyf14); Natural Science Foundation of China (82072026, 82072025 and 82272090); Zhejiang Provincial Natural Science Foundation (LY23H180003, LQ22H180010); Provincial and Ministerial Joint Construction of Key Projects (WKJ-ZJ-2317).

## Supplementary materials

Supplementary material associated with this article can be found, in the online version, at doi:10.1016/j.ajps.2024.100905.

## REFERENCES

- Giaquinto AN, Sung H, Miller KD, Kramer JL, Newman LA, Minihan A, et al. Breast cancer statistics, 2022. *CA Cancer J Clin* 2022;72(6):524–41.
- Zhang Y, Pan H, Yu C, Liu R, Xing B, Jia B, et al. Phytoestrogen-derived multifunctional ligands for targeted therapy of breast cancer. *Asian J Pharm Sci* 2023;18(4):100827.
- Sung H, Ferlay J, Siegel RL, Laversanne M, Soerjomataram I, Jemal A, et al. Global cancer statistics 2020: GLOBOCAN estimates of incidence and mortality worldwide for 36 cancers in 185 countries. *CA Cancer J Clin* 2021;71(3):209–49.
- Yin L, Duan JJ, Bian XW, Yu SC. Triple-negative breast cancer molecular subtyping and treatment progress. *Breast Cancer Res* 2020;22(1):61.
- Obidiro O, Battogtokh G, Akala EO. Triple negative breast cancer treatment options and limitations: future outlook. *Pharmaceutics* 2023;15(7):1796.
- Chapdelaine AG, Sun G. Challenges and opportunities in developing targeted therapies for triple negative breast cancer. *Biomolecules* 2023;13(8):1207.
- Berger ER, Park T, Saridakis A, Golshan M, Greenup RA, Ahuja N. Immunotherapy treatment for triple negative breast cancer. *Pharmaceutics* 2021;14(8):763.
- Bianchini G, De Angelis C, Licata L, Gianni L. Treatment landscape of triple-negative breast cancer - expanded options, evolving needs. *Nat Rev Clin Oncol* 2022;19(2):91–113.
- Chabner BA, Roberts TG Jr. Timeline: chemotherapy and the war on cancer. *Nat Rev Cancer* 2005;5(1):65–72.
- Mahoutforoush A, Solouk A, Hamishehkar H, Haghbin Nazarpak M, Abbaspour-Ravasjani S. Novel decorated nanostructured lipid carrier for simultaneous active targeting of three anti-cancer agents. *Life Sci* 2021;279:119576.
- Galluzzi L, Humeau J, Buqué A, Zitvogel L, Kroemer G. Immunostimulation with chemotherapy in the era of immune checkpoint inhibitors. *Nat Rev Clin Oncol* 2020;17(12):725–41.
- Wang C, Yu H, Yang X, Zhang X, Wang Y, Gu T, et al. Elaborately engineering of a dual-drug co-assembled nanomedicine for boosting immunogenic cell death and enhancing triple negative breast cancer treatment. *Asian J Pharm Sci* 2022;17(3):412–24.
- Qi J, Jin F, You Y, Du Y, Liu D, Xu X, et al. Synergistic effect of tumor chemo-immunotherapy induced by leukocyte-hitchhiking thermal-sensitive micelles. *Nat Commun* 2021;12(1):4755.
- Zhou J, Wang G, Chen Y, Wang H, Hua Y, Cai Z. Immunogenic cell death in cancer therapy: present and emerging inducers. *J Cell Mol Med* 2019;23(8):4854–65.
- Galluzzi L, Buqué A, Kepp O, Zitvogel L, Kroemer G. Immunogenic cell death in cancer and infectious disease. *Nat Rev Immunol* 2017;17(2):97–111.
- Obeid M, Tesniere A, Ghiringhelli F, Fimia GM, Apetoh L, Perfettini JL, et al. Calreticulin exposure dictates the immunogenicity of cancer cell death. *Nat Med* 2007;13(1):54–61.
- Yong SB, Ramishetti S, Goldsmith M, Diesendruck Y, Hazan-Halevy I, Chatterjee S, et al. Dual-targeted lipid nanotherapeutic boost for chemo-immunotherapy of cancer. *Adv Mater* 2022;34(13):e2106350.
- Heinhuis KM, Ros W, Kok M, Steeghs N, Beijnen JH, Schellens JHM. Enhancing antitumor response by combining immune checkpoint inhibitors with chemotherapy in solid tumors. *Ann Oncol* 2019;30(2):219–35.
- Fan Q, Chen Z, Wang C, Liu Z. Toward biomaterials for enhancing immune checkpoint blockade therapy. *Adv Funct Mater* 2018;28(37):1802540.
- Sun Y, Feng X, Wan C, Lovell JF, Jin H, Ding J. Role of nanoparticle-mediated immunogenic cell death in cancer immunotherapy. *Asian J Pharm Sci* 2021;16(2):129–32.
- Sun Y. Tumor microenvironment and cancer therapy resistance. *Cancer Lett* 2016;380(1):205–15.
- Petitprez F, Meylan M, de Reyniès A, Sautès-Fridman C, Fridman WH. The tumor microenvironment in the response to immune checkpoint blockade therapies. *Front Immunol* 2020;11:784.
- Wang JX, Choi SYC, Niu X, Kang N, Xue H, Killam J, et al. Lactic acid and an acidic tumor microenvironment suppress anticancer immunity. *Int J Mol Sci* 2020;21(21).
- Meng X, Xu Y, Lu Q, Sun L, An X, Zhang J, et al. Ultrasound-responsive alkaline nanorobots for the treatment of lactic acidosis-mediated doxorubicin resistance. *Nanoscale* 2020;12(25):13801–10.
- Abumanhal-Masarweh H, Koren L, Zinger A, Yaari Z, Krinsky N, Kaneti G, et al. Sodium bicarbonate nanoparticles modulate the tumor pH and enhance the cellular uptake of doxorubicin. *J Control Release* 2019;296:1–13.
- Chen M, Guo X, Shen L, Ding J, Yu J, Chen X, et al. Monodisperse CaCO<sub>3</sub>-loaded gelatin microspheres for reversing lactic acid-induced chemotherapy resistance during TACE treatment. *Int J Biol Macromol* 2023;231:123160.
- Jain RK. Normalization of tumor vasculature: an emerging concept in antiangiogenic therapy. *Science* 2005;307(5706):58–62.
- Kirtane AR, Kalscheuer SM, Panyam J. Exploiting nanotechnology to overcome tumor drug resistance: challenges and opportunities. *Adv Drug Deliv Rev* 2013;65(13–14):1731–47.
- Minassian LM, Cotechini T, Huitema E, Graham CH. Hypoxia-induced resistance to chemotherapy in cancer. *Adv Exp Med Biol* 2019;1136:123–39.
- Singleton DC, Macann A, Wilson WR. Therapeutic targeting of the hypoxic tumour microenvironment. *Nat Rev Clin Oncol* 2021;18(12):751–72.
- Romero-Garcia S, Moreno-Altamirano MM, Prado-Garcia H, Sánchez-García FJ. Lactate contribution to the tumor microenvironment: mechanisms, effects on immune cells and therapeutic relevance. *Front Immunol* 2016;7:52.
- Wang JX, Choi SY, Niu X, Kang N, Xue H, Killam J, et al. Lactic acid and an acidic tumor microenvironment suppress anticancer immunity. *Int J Mol Sci* 2020;21(21):8363.
- Yang J, Li W, Luo L, Jiang M, Zhu C, Qin B, et al. Hypoxic tumor therapy by hemoglobin-mediated drug delivery and

- reversal of hypoxia-induced chemoresistance. *Biomaterials* 2018;182:145–56.
- [34] Yang Z, Zhu Y, Dong Z, Li W, Yang N, Wang X, et al. Tumor-killing nanoreactors fueled by tumor debris can enhance radiofrequency ablation therapy and boost antitumor immune responses. *Nat Commun* 2021;12(1):4299.
- [35] Zhang YX, Zhao YY, Shen J, Sun X, Liu Y, Liu H, et al. Nanoenabled modulation of acidic tumor microenvironment reverses anergy of infiltrating T cells and potentiates anti-PD-1 therapy. *Nano Lett* 2019;19(5):2774–83.
- [36] Lv J, Wang X, Zhang X, Xu R, Hu S, Wang S, et al. Tumor microenvironment-responsive artesunate loaded Z-scheme heterostructures for synergistic photo-chemodynamic therapy of hypoxic tumor. *Asian J Pharm Sci* 2023;18(3):100798.
- [37] Meng Z, Zhou X, Xu J, Han X, Dong Z, Wang H, et al. Light-triggered in situ gelation to enable robust photodynamic-immunotherapy by repeated stimulations. *Adv Mater* 2019;31(24):e1900927.
- [38] Zhu Y, Yang Z, Dong Z, Gong Y, Hao Y, Tian L, et al. CaCO<sub>3</sub>-assisted preparation of pH-responsive immune-modulating nanoparticles for augmented chemo-immunotherapy. *Nanomicro Lett* 2020;13(1):29.
- [39] Wang GL, Jiang BH, Rue EA, Semenza GL. Hypoxia-inducible factor 1 is a basic-helix-loop-helix-PAS heterodimer regulated by cellular O<sub>2</sub> tension. *Proc Natl Acad Sci USA* 1995;92(12):5510–14.
- [40] Shu G, Chen M, Song J, Xu X, Lu C, Du Y, et al. Sialic acid-engineered mesoporous polydopamine nanoparticles loaded with SPIO and Fe<sup>3+</sup> as a novel theranostic agent for T1/T2 dual-mode MRI-guided combined chemo-photothermal treatment of hepatic cancer. *Bioact Mater* 2021;6(5):1423–35.
- [41] Zhu M, Zhu L, You Y, Sun M, Jin F, Song Y, et al. Positive chemotaxis of CREKA-modified ceria@polydopamine biomimetic nanoswimmers for enhanced penetration and chemo-photothermal tumor therapy. *ACS Nano* 2023;17(17):17285–98.
- [42] Li Q, Chen Y, Zhou X, Chen D, Li Y, Yang J, et al. Hyaluronic acid–methotrexate conjugates coated magnetic polydopamine nanoparticles for multimodal imaging-guided multistage targeted chemo-photothermal therapy. *Mol Pharmaceut* 2018;15(9):4049–62.
- [43] Shu G, Lu C, Wang Z, Du Y, Xu X, Xu M, et al. Fucoidan-based micelles as P-selectin targeted carriers for synergistic treatment of acute kidney injury. *Nanomedicine* 2021;32:102342.
- [44] Han H, Li S, Zhong Y, Huang Y, Wang K, Jin Q, et al. Emerging pro-drug and nano-drug strategies for gemcitabine-based cancer therapy. *Asian J Pharm Sci* 2022;17(1):35–52.
- [45] Huang P, Qian X, Chen Y, Yu L, Lin H, Wang L, et al. Metalloporphyrin-encapsulated biodegradable nanosystems for highly efficient magnetic resonance imaging-guided sonodynamic cancer therapy. *J Am Chem Soc* 2017;139(3):1275–84.
- [46] Hao Y, Chen M, Wu Y, Dong Z, Zhu Y, Wang C, et al. CaCO<sub>3</sub> based proton nanosponge to potentiate immune checkpoint blockade therapy by synergistically reversing tumor immunosuppression. *Chem Eng J* 2023;462:142206.
- [47] Ding Y, Wang Y, Hu Q. Recent advances in overcoming barriers to cell-based delivery systems for cancer immunotherapy. *Exploration* 2022;2(3):20210106.